




Observational Evidence for Self-generation of Small-scale Magnetic Flux Ropes from Intermittent Solar Wind Turbulence

Jinlei Zheng¹ and Qiang Hu² 

¹ Department of Space Science, The University of Alabama in Huntsville, Huntsville, AL 35805, USA

² Department of Space Science and CSPAR, The University of Alabama in Huntsville, Huntsville, AL 35805, USA; qiang.hu.th@dartmouth.edu, qh0001@uah.edu

Received 2017 November 15; revised 2017 December 20; accepted 2017 December 22; published 2018 January 5

Abstract

We present unique and additional observational evidence for the self-generation of small-scale coherent magnetic flux rope structures in the solar wind. Such structures with durations between 9 and 361 minutes are identified from *Wind* in situ spacecraft measurements through the Grad–Shafranov (GS) reconstruction approach. The event occurrence counts are on the order of 3500 per year on average and have a clear solar-cycle dependence. We build a database of small-scale magnetic flux ropes from 20 yr worth of *Wind* spacecraft data. We show a power-law distribution of the wall-to-wall time corresponding well to the inertial range turbulence, which agrees with relevant observations and numerical simulation results. We also provide the axial current density distribution from the GS-based observational analysis, which yields a non-Gaussian probability density function consistent with numerical simulation results.

Key words: magnetic fields – magnetohydrodynamics (MHD) – methods: data analysis – plasmas – solar wind – turbulence

1. Introduction

Small-scale magnetic flux ropes in the solar wind of durations ranging from a few minutes to a few hours have been identified from in situ spacecraft data and studied for decades (e.g., Moldwin et al. 1995, 2000; Feng et al. 2008; Cartwright & Moldwin 2010; Yu et al. 2014). They possess some similar features in magnetic field configurations to their large-scale counterparts, the magnetic clouds (MCs) of durations lasting for a dozen hours up to a few days, but differ in certain plasma properties. Unlike MCs, which have a clear solar origin related to coronal mass ejections, the origin of these small-scale magnetic flux ropes is still debated. One view is that they also have a solar source correspondence, especially for intermediate-sized flux ropes (e.g., Feng et al. 2008), based on some similar statistical properties as MCs. As advocated by Borovsky (2008), the “flux tubes” bounded by discontinuities may be rooted on the Sun, permeating the whole interplanetary space. The other view, supported not only by observational analysis, but also extensively by numerical simulations over a wide range of scales (Servidio et al. 2008; Greco et al. 2008, 2009a, 2009b, 2010; Wan et al. 2013, 2015), states that the generation process of small-scale magnetic flux ropes or islands in strict two-dimensional (2D) configuration is intrinsic to magnetohydrodynamic (MHD) turbulence often approximated by a quasi-2D model or containing a dominant 2D component (e.g., Matthaeus et al. 2007; Zank et al. 2017, and references therein). They are believed to be the byproduct of the solar wind turbulence dynamic evolution process, resulting in the generation of coherent structures including “small random current,” “current cores,” and “current sheets” (Greco et al. 2009a) over the inertial range length scales.

Accompanying these studies associated with small-scale flux ropes, the observational analysis on the discontinuities or current sheets possibly bounding the flux ropes (or flux tubes; see, e.g., Borovsky 2008) is also ongoing. Various approaches have been utilized to identify these structures mostly as incremental changes in the magnetic field from in situ

time-series data (e.g., Bruno et al. 2001; Vasquez et al. 2007; Borovsky 2008; Greco et al. 2009a, 2010; Miao et al. 2011; Osman et al. 2014; Greco et al. 2016). However, there is generally a lack of synergy between the analyses of these two types of coherent structures, and the analysis method for the small-scale magnetic flux ropes is outdated. In this Letter, we explore the application of the Grad–Shafranov (GS) reconstruction technique to the automated detection of small-scale magnetic flux ropes for the first time. Meanwhile, we report on the successful identification of an unprecedented number of the small-scale flux rope events via the GS approach and associated analysis results including unique physical characterization of these structures, especially the axial current density distribution, which enables a direct comparison with the numerical simulation results for 2D MHD turbulence. To the best of our knowledge, the estimate of current density has to be achieved by using closely spaced multiple spacecraft through the curlometer approach, such as from the Cluster and Magnetospheric Multiscale (MMS) missions (see, e.g., Greco et al. 2018, for such a comparison of current density between MMS measurements and 2D simulations).

The GS reconstruction technique is based on the GS equation, describing 2D (or 2.5D with non-vanishing axial magnetic field) cylindrical magnetic field and plasma configurations in magnetohydrostatic equilibrium (see Hu 2017 for a comprehensive review) that is more general than the force-free assumption. For the magnetic field components $\mathbf{B} = (\partial A/\partial y, -\partial A/\partial x, B_z(A))$ defined by the 2D magnetic flux function $A(x, y)$ in Cartesian coordinates (with z -axis along the flux rope axis, and $\partial/\partial z \approx 0$), the transverse force balance yields the GS equation (reduced from the usual equation $\nabla p = \mathbf{J} \times \mathbf{B}$),

$$\frac{\partial^2 A}{\partial x^2} + \frac{\partial^2 A}{\partial y^2} = -\mu_0 \frac{dP_t}{dA} = -\mu_0 J_z(A). \quad (1)$$

Here the right-hand side gives the axial current density J_z which is a total derivative of the transverse pressure

$P_t = p + B_z^2/2\mu_0$, the sum of the plasma pressure and the axial magnetic pressure, with respect to A . All of these quantities can be evaluated along a single-spacecraft path across a flux rope structure. Since the flux function A characterizes the nested cylindrical flux surfaces of a flux rope, the axial current density distribution throughout such a flux rope configuration is readily obtained by the function $J_z(A)$ determined from in situ spacecraft data. Additionally, the cross section of a cylindrical flux rope given by the solution $A(x, y)$ to the GS equation over a rectangular domain can also be obtained numerically (Hu & Sonnerup 2001, 2002). The technique has been widely applied to reconstruct structures in a variety of space plasma regimes (see, e.g., Hu 2017). The application of the GS method to the small-scale structures of relevance to the quasi-2D MHD turbulence as envisaged by Matthaeus et al. (2007) has just begun.

Telloni et al. (2016) took yet another approach by evaluating the MHD rugged invariants (see also, Telloni et al. 2013) within about 144 flux ropes identified in prior studies. They concluded that flux ropes represent well-organized structures coming from the dynamical evolution of the MHD turbulent cascade, in which the MHD invariants are inter-related. They further stated that the flux ropes dynamically evolve toward a final steady state in which the (normalized) magnetic helicity σ_m , and cross-helicity σ_c values within the structures are distributed according to $\sigma_m^2 + \sigma_c^2 = 1$. We expect to complement that study by providing a more exhaustive list of events equipped with more comprehensive characterizations of flux rope properties. For instance, from the GS reconstruction output, we will be able to derive, quantitatively and directly, the total magnetic energy, magnetic flux, and (relative) magnetic helicity (Hu 2017) contained in each flux rope, although this is not the focus of the current analysis, and we have excluded Alfvénic structures or structures with high Alfvénicity.

We present and briefly introduce the small-scale flux rope database built by an automated process based on the GS method in the next section. In Section 3, we present the analysis results of the wall-to-wall time and the axial current density distributions derived from our database and compare them directly with Greco et al. (2009a). We conclude in the last section, and signify the uniqueness of our approach and result in support of the view of the self-generation of small-scale flux ropes via MHD turbulence.

2. Small-scale Flux Rope Database via the GS Reconstruction Method

We have built a small-scale magnetic flux rope database via the GS reconstruction method. The GS method was first applied to reconstruct cross sections of small-scale magnetic flux ropes in the solar wind with durations of about half an hour in Hu & Sonnerup (2001). In the present study, we apply to *Wind* in situ spacecraft measurements of 1 minute cadence between 1996 and 2016, based on largely the same principles and procedures without carrying out the final numerical reconstruction of solving for a 2D solution to the GS equation on the cross-sectional plane. Detailed descriptions of the automated detection algorithm including a flowchart illustrating the step-by-step implementation of the GS-based algorithm are presented in Zheng (2017).

Table 1
Metrics and Selection Criteria for the GS-based Automated Flux Rope Detection Algorithm

Duration (minutes)	\bar{B} (nT)	RES	R_f	Walén Slope
9 ~ 361	≥ 5	≤ 0.12	≤ 0.14	≤ 0.3

In short, the detection procedures start by sliding a rectangular window of a chosen width through the time series to select the data interval for analysis. For each interval and the selected magnetic field and plasma parameters, the same procedures apply as the standard GS reconstruction of 2.5D magnetohydrostatic structures. The main steps are to obtain the flux function A and the transverse pressure P_t values along the spacecraft path in a properly determined trial frame of reference (Hu & Sonnerup 2002). Then the necessary conditions for a 2.5D cylindrical magnetic flux rope configuration, mainly the requirement that the function $P_t(A)$ be single-valued based on the GS equation and the double-folding pattern in A across the flux rope characteristic of nested closed flux surfaces (each of a distinct A value), are checked by producing a set of quantitative metrics. After a trial-and-error process, especially by enumerating all the possible z -axis orientations in its parameter space, the set of metrics is obtained and a flux rope candidate is positively identified if the selection threshold conditions are satisfied, as indicated in Table 1. The flux rope interval is then identified and recorded with a size/duration limited by the width of the data window. Flux ropes with different sizes are simply identified by iterations, repeating the aforementioned procedures with different-width sliding windows. Additional post-processing procedures are taken to clean up overlapping intervals and to ensure good-quality events in our database according to the additional metrics in Table 1. In summary, the two metrics, RES and R_f , originally defined in Hu & Sonnerup (2002) and Hu et al. (2004), respectively, evaluate the quality of $P_t(A)$ being single-valued and each has to be smaller than the specific threshold. The Walén slope (Paschmann & Sonnerup 2008), corresponding to the average ratio between the remaining plasma flow (ideally zero) in the frame of reference moving with the flux rope and the local Alfvén velocity, is used as a criterion to remove Alfvénic structures. We also have the option to restrict our database to only contain flux ropes of average magnetic field magnitude $\bar{B} \geq 5$ nT, following the previous studies (e.g., Cartwright & Moldwin 2010) and avoiding complications due to low Alfvén speed, in the present study. Therefore, our database contains the small-scale flux ropes with helical magnetic field configuration and negligible remaining plasma flow, corresponding to $\sigma_c \approx 0$ and the maximum $\sigma_m \approx \pm 1$ as expected based on Telloni et al. (2016). However, our database contains events with a wide range of plasma (proton) β values, yielding both a mean and a median around 0.5, since we are not limited to finding low- β structures only.

We have identified a total number of 74,241 distinct small-scale magnetic flux rope events with durations ranging from 9 to 361 minutes from the *Wind* spacecraft data sets. We have summarized and compiled our detection results onto a publicly available website, <http://fluxrope.info>, which contains some essential information about the properties of the detected flux rope structures. Various statistical analyses have been performed and reported in Zheng (2017). At a glimpse, Figure 1 presents the monthly event counts in our database,

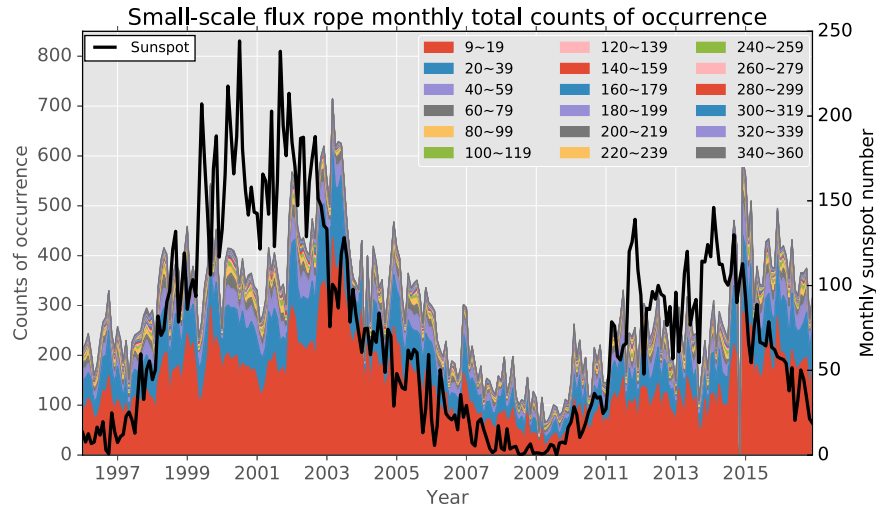


Figure 1. Monthly counts (left axis) of small-scale magnetic flux rope events identified from *Wind* in situ spacecraft measurements during 1996–2016. The counts are separated for flux ropes of different durations and color-coded as indicated by the legends in minutes. The corresponding monthly sunspot numbers are given by the black curve (right axis).

covering the past two solar cycles. Clearly the total counts, including all events of variable durations follow the monthly sunspot numbers, hinting at solar-cycle dependency of their occurrence. The events of smaller durations generally have greater rates of occurrence. The peaks of occurrence counts tend to appear in the declining phase of each solar cycle. On average, we have identified more than 3500 small-scale magnetic flux ropes per year. We caution, however, against a quick conclusion about the solar origin of these structures, because we believe there should be a distinction between “solar origin” and “solar activity dependence” as indicated by the dependence on sunspot numbers for the latter. In addition, some local turbulence processes could also be modulated by the solar activity, leading to the solar-cycle dependence as exhibited here. For example, perhaps the simplest case was the modulation of cosmic-ray transport coefficients by the solar-cycle variations in the magnetic field magnitude and variance (Manuel et al. 2011). Furthermore, the recent works of Zhao et al. (2017) and L.-L. Zhao et al. (2018, in preparation) showed the solar-cycle dependence of various turbulence quantities affecting cosmic-ray diffusion, such as Elsässer variables, correlation lengths, and residue energy, etc. They are all derived locally and with contributions from local driving sources, based on sophisticated MHD turbulence theory (Adhikari et al. 2014; Zank et al. 2017).

3. Wall-to-Wall Time and Axial Current Density Distributions

With such a small-scale magnetic flux rope database, we are positioned to perform detailed statistical analysis in addition to the occurrence rate distribution demonstrated in Figure 1. We report here important findings about the wall-to-wall time and the axial current density J_z distributions from the identified flux ropes. They have direct and significant relevance to the findings of Greco et al. (2009a).

The results from our analysis are presented in Figures 2 and 3. The current density is derived from dP_t/dA , as indicated in Equation (1), where both P_t and A are evaluated from in situ spacecraft measurements for each individual event. To facilitate a direct comparison with the numerical simulation result, which is 2D in nature (Greco et al. 2009a), we calculated the axial

current density samples in each event at a rate proportional to its scale size and congregated the results together from all events. The flux rope wall-to-wall time is simply the distribution by putting together the flux rope duration and the separation time in-between adjacent flux rope intervals. The flux rope wall or boundary in our database is considered as a type of discontinuity (see, e.g., Borovsky 2008) or current sheet. Therefore, the wall-to-wall time in our analysis is used as a proxy to the waiting time between current sheets or discontinuities of negligible thicknesses. Such waiting time distributions (WTDs) have been analyzed in a number of previous works (e.g., Bruno et al. 2001; Vasquez et al. 2007; Greco et al. 2008, 2009a, 2009b; Miao et al. 2011) by directly identifying current sheets or discontinuities from in situ time-series data. We note that our proxy is unique and valid for flux ropes bounded by discontinuities broadly defined as locations where the magnetic field and/or plasma parameters change. This is consistent with our choice of flux rope boundaries based on the GS method (Hu et al. 2004). They are chosen as the locations along the approximately single-valued and double-folded P_t versus A curve, corresponding to the specific data points in the time series of both the magnetic field and plasma measurements. Beyond those points, i.e., beyond the flux rope boundary, the data, in terms of $P_t = p + B_z^2/2\mu_0$ as a function of A , start to deviate. This often corresponds to the concurrent changes or increments in magnetic field and plasma parameters when a flux-tube (or rope) boundary is encountered (Borovsky 2008). Therefore, this lends to the justification for using the wall-to-wall time as a proxy to the current-sheet waiting time.

Figure 2 shows the wall-to-wall time distribution of small-scale flux ropes. The distribution is well fitted by two power-law functions of different power indices as indicated, with a break point located at ~ 60 minutes. The outliers near the two ends are due to the cutoff effect of limited durations for these events. The WTDs of the observed solar wind discontinuities in Greco et al. (2009a) showed a power law within the break point at ~ 50 minutes, corresponding to the typical correlation length scale (Matthaeus et al. 2005), which is consistent with our result. In addition, the power-law index from Greco et al. (2009b) is -0.92 ± 0.03 from the numerical simulation, and -1.23 ± 0.03 from the in situ spacecraft observations at 1 au,

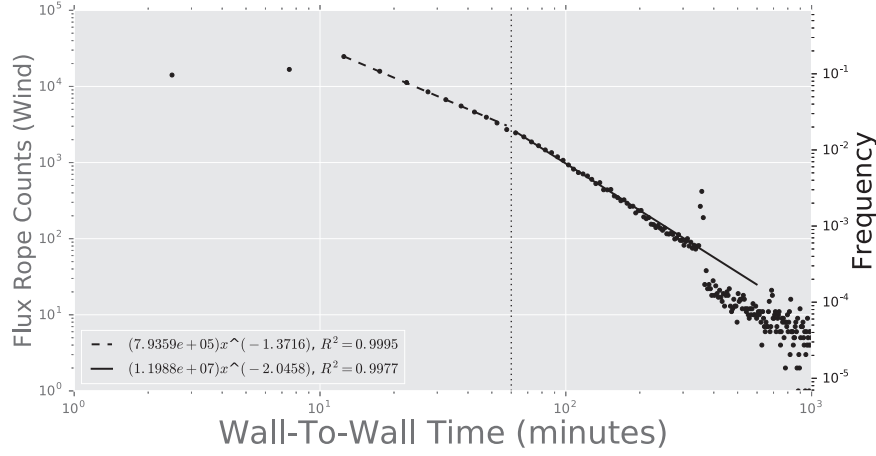


Figure 2. Wall-to-wall time distribution of small-scale flux ropes in our database. The dashed and solid black lines are the power-law fittings to the two sections divided by the dotted line at 60 minutes. The fitting parameters are denoted, for each line, in the lower left corner with the goodness-of-fit parameter R^2 , the coefficient of determination.

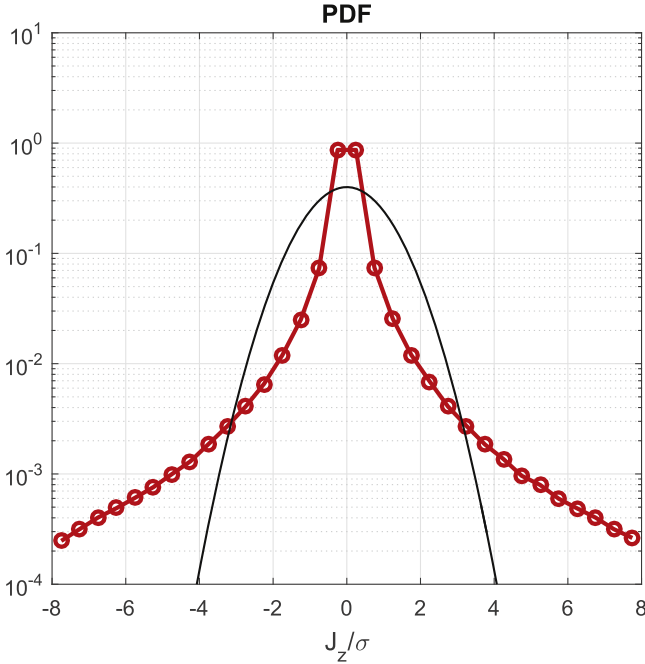


Figure 3. Probability density function (PDF) of the axial current density J_z distribution associated with magnetic flux ropes normalized by the standard deviation σ ($\sigma = 8.42 \times 10^{-11}$ A/m²). The thin black curve is the standard Gaussian distribution with unit variance.

for the range below the break point, i.e., in the inertial range of solar wind turbulence. They compare well with our result, -1.37 for the dashed black line in Figure 2. We note that for the case including additional flux rope events by relaxing the criterion on \bar{B} to $\bar{B} > 0$, the number of events doubles and the power-law fitting to the wall-to-wall time persists. The index for the inertial range becomes -1.22 . The section beyond the break point can still be fitted by a power-law function with a power index ~ -2 . However, the interpretation of this portion is not certain and has yet to be improved with better statistics.

Figure 3 shows the PDF of the normalized axial current density distribution inside and near the boundaries of the small-scale magnetic flux ropes in our database, in the same format as the result presented by Greco et al. (2009a) from the 2D MHD simulation. They also characterized their non-Gaussian PDF by

three regions: regions I and III are super-Gaussian, around the center and toward the tails of the PDF, corresponding to current-sheet-like structures in-between magnetic flux ropes or magnetic islands, but with the weakest and strongest current density in magnitude, respectively; region II corresponds to the sub-Gaussian section with modest magnitude of current density, mostly appearing inside flux rope cores. Our result in Figure 3 exhibits the same general non-Gaussian features in agreement with Greco et al. (2009a).

4. Conclusions

In conclusion, in this Letter, we report the analysis result of the wall-to-wall time and axial current density distributions from in situ spacecraft observations of small-scale magnetic flux ropes based on an extensive event database and the unique GS model output. Our results show a power-law distribution of the wall-to-wall time for length scales smaller than the correlation length, corresponding well to the inertial range of solar wind turbulence. This result is consistent with the analysis result of Greco et al. (2009a) from both observational analyses using an entirely different approach and MHD simulations of intermittent turbulence. In addition, we also obtain the non-Gaussian distribution of the axial current density associated with the magnetic flux ropes, which is also in agreement with the numerical simulation result of Greco et al. (2009a). We therefore conclude that we have provided unique and additional observational evidence in support of the view of self-generation of coherent structures, such as small-scale magnetic flux ropes and current sheets, locally from MHD turbulence. In light of the analysis by Telloni et al. (2016), we plan to extend our analysis to include structures of significant remaining flow, i.e., structures with $\sigma_c \neq 0$. This is feasible since the extension of the GS method to the GS-type with significant field-aligned flow and even to the 2D MHD equilibrium has been developed (see Hu 2017). Meanwhile, we also invite other researchers to extend their relevant studies by utilizing our extensive database.

We are grateful to our colleagues, Drs. Laxman Adhikari, Jakobus le Roux, Gang Li, Gary Webb, Gary Zank, and Lingling Zhao for illuminating discussions and suggestions that have made this work possible. We acknowledge NASA grants

NNX12AH50G, NNX14AF41G, NNX17AB85G, subawards NRL N00173-14-1-G006 and SAO SV4-84017, and NSF grant AGS-1650854 for support. We thank Drs. M. G. Linton and P. Riley for stimulating discussions on the GS-based flux rope identification, which initiated this work. We also thank the reviewer for expert comments and suggestions.

ORCID iDs

Qiang Hu  <https://orcid.org/0000-0002-7570-2301>

References

- Adhikari, L., Zank, G. P., Hu, Q., & Dosch, A. 2014, *ApJ*, **793**, 52
- Borovsky, J. E. 2008, *JGRA*, **113**, A08110
- Bruno, R., Carbone, V., Veltri, P., Pietropaolo, E., & Bavassano, B. 2001, *P&SS*, **49**, 1201
- Cartwright, M. L., & Moldwin, M. B. 2010, *JGRA*, **115**, A08102
- Feng, H. Q., Wu, D. J., Lin, C. C., et al. 2008, *JGRA*, **113**, A12105
- Greco, A., Chuychai, P., Matthaeus, W. H., Servidio, S., & Dmitruk, P. 2008, *GeoRL*, **35**, 119111
- Greco, A., Matthaeus, W. H., Perri, S., et al. 2018, *SSRv*, **214**, 1
- Greco, A., Matthaeus, W. H., Servidio, S., Chuychai, P., & Dmitruk, P. 2009a, *ApJL*, **691**, L111
- Greco, A., Matthaeus, W. H., Servidio, S., & Dmitruk, P. 2009b, *PhRvE*, **80**, 046401
- Greco, A., Perri, S., Servidio, S., Yordanova, E., & Veltri, P. 2016, *ApJL*, **823**, L39
- Greco, A., Servidio, S., Matthaeus, W. H., & Dmitruk, P. 2010, *P&SS*, **58**, 1895
- Hu, Q. 2017, *Sci. China Earth Sci.*, **60**, 1466
- Hu, Q., Smith, C. W., Ness, N. F., & Skoug, R. M. 2004, *JGRA*, **109**, A03102
- Hu, Q., & Sonnerup, B. U. Ö 2001, *GeoRL*, **28**, 467
- Hu, Q., & Sonnerup, B. U. Ö. 2002, *JGRA*, **107**, 1142
- Manuel, R., Ferreira, S., Potgieter, M., Strauss, R., & Engelbrecht, N. 2011, *AdSpR*, **47**, 1529
- Matthaeus, W. H., Bieber, J. W., Ruffolo, D., Chuychai, P., & Minnie, J. 2007, *ApJ*, **667**, 956
- Matthaeus, W. H., Dasso, S., Weygand, J. M., et al. 2005, *PhRvL*, **95**, 231101
- Miao, B., Peng, B., & Li, G. 2011, *AnGeo*, **29**, 237
- Moldwin, M. B., Ford, S., Lepping, R., Slavin, J., & Szabo, A. 2000, *GeoRL*, **27**, 57
- Moldwin, M. B., Phillips, J. L., Gosling, J. T., et al. 1995, *JGRA*, **100**, 19903
- Osman, K. T., Matthaeus, W. H., Gosling, J. T., et al. 2014, *PhRvL*, **112**, 215002
- Paschmann, G., & Sonnerup, B. U. Ö. 2008, *ISSIR*, **8**, 65
- Servidio, S., Matthaeus, W. H., & Dmitruk, P. 2008, *PhRvL*, **100**, 095005
- Telloni, D., Carbone, V., Perri, S., et al. 2016, *ApJ*, **826**, 205
- Telloni, D., Perri, S., Bruno, R., Carbone, V., & Amicis, R. D. 2013, *ApJ*, **776**, 3
- Vasquez, B. J., Abramenko, V. I., Haggerty, D. K., & Smith, C. W. 2007, *JGRA*, **112**, A11102
- Wan, M., Matthaeus, W. H., Roytershteyn, V., et al. 2015, *PhRvL*, **114**, 175002
- Wan, M., Matthaeus, W. H., Servidio, S., & Oughton, S. 2013, *PhPl*, **20**, 042307
- Yu, W., Farrugia, C. J., Lugaz, N., et al. 2014, *JGR*, **119**, 689
- Zank, G. P., Adhikari, L., Hunana, P., et al. 2017, *ApJ*, **835**, 147
- Zhao, L.-L., Adhikari, L., Zank, G. P., Hu, Q., & Feng, X. S. 2017, *ApJ*, **849**, 88
- Zheng, J. 2017, PhD thesis, The Univ. of Alabama in Huntsville